

Abundances in planetary nebulae: Mz 3[★]

S. R. Pottasch¹ and R. Surendiranath²

¹ Kapteyn Astronomical Institute, PO Box 800, 9700 AV Groningen, The Netherlands
e-mail: pottasch@astro.rug.nl

² Indian Institute of Astrophysics, Koramangala II Block, Bangalore 560034, India

Received 20 May 2005 / Accepted 22 August 2005

ABSTRACT

ISO spectra of the bipolar planetary nebula Mz 3 are used to determine the element abundances in the bright lobes of the nebula. The ISO spectra alone are sufficient to determine nitrogen, neon, argon, sulfur and iron abundances. These spectra are combined with spectra in the visual wavelength region (taken from the literature) to obtain an extinction corrected spectrum which is used to determine the abundance of oxygen and some other elements using a classical determination. We have tried abundance determination using photoionization modeling using CLOUDY, which is essential for determining the helium, silicon and chlorine abundances. It was found difficult to model the entire spectrum. New information about the central star could be determined. The abundances determined are found to differ somewhat from earlier results using only visual spectra. The reasons for this difference are discussed. An elevated helium abundance is found, agreeing with the determination of Smith 2003. Taken together with the high nitrogen abundance found, it is concluded that the exciting star of Mz 3 had a high progenitor mass.

Key words. ISM: abundances – stars: AGB and post-AGB – planetary nebulae: individual: Mz 3

1. Introduction

Mz 3 (Menzel 3) is an intrinsically bright young bipolar planetary nebula (PN 331.7-01.0). It extends for more than 50'' along its major axis, although its two bright polar lobes extend about 12'' in an almost north-south direction on either side of its bright unresolved nucleus. It has been well studied in recent years. The visual and infrared spectrum has been studied by Zhang & Liu (2002), by Smith (2003) and by Smith & Gehrz (2005). A radio interferometric study of the nebula at four wavelengths between 3.5 cm and 21 cm has been made by Bains et al. (2004); the 6 cm flux density they find, about 630 mJy indicates that the nebula is one of the strongest emission sources in the sky. It is therefore reasonably close although there is no reliable estimate of its distance.

Narrow band HST images of the nebula have been studied by Guerrero et al. (2004) and Santander-Garcia et al. (2004). It is clearly a very complicated nebula. Besides the bright inner lobes, there are also cylindrical and conical lobes and an equatorial ellipse. These structures extend much further than the bright conical lobes and are at a much lower intensity level. None of these additional structures is seen in the radio maps of Bains et al. (2004). In this paper we concern ourselves only with the bright inner lobes and the central source.

The nebula is located close to the galactic plane, in a region of the sky with a rather high extinction. It is difficult to obtain an exact value of the extinction but in this direction it probably lies between 1 and 2 mag/kpc (see e.g. Lucke 1978). The extinction of the nebula is rather high: much of it is interstellar but some of it is local to the nebula. We shall discuss this presently. Here we may note one of the consequences of the high extinction: the attempt at obtaining an IUE spectrum of the nebula produced a very noisy and unusable spectrum, although other nebulae which are even weaker radio sources produced good IUE spectra with the same observing time.

We have earlier studied nebulae with bilobal structure which at first sight appear similar to Mz 3. These are NGC 6357 (Pottasch et al. 2000) and Hb5 (unpublished). Besides the bilobal structure both of these nebulae have a bright central source which is also nebular. In these two cases however most of the emission comes from the central nebula and the lobes make only a negligible contribution to the total emission. In Mz 3 it is the lobes which make the largest contribution to the total emission although the contribution of the central source is not negligible. It may be that Mz 3 is a younger version of these three nebulae. There are two reasons for this supposition. Firstly because the temperature of the central star is rather low (between 35 000 K and 40 000 K) compared to well over 100 000 K for the other two nebulae. Secondly because the electron density is very high in the central nebula of Mz 3, over 10^6 cm^{-3} , i.e. at least two orders of magnitude higher than in the central source of the two other nebulae. In Mz 3 it is the

[★] Based on observations with ISO, an ESA project with instruments funded by ESA Member States (especially the PI countries: France, Germany, the Netherlands and the United Kingdom) and with the participation of ISAS and NASA.

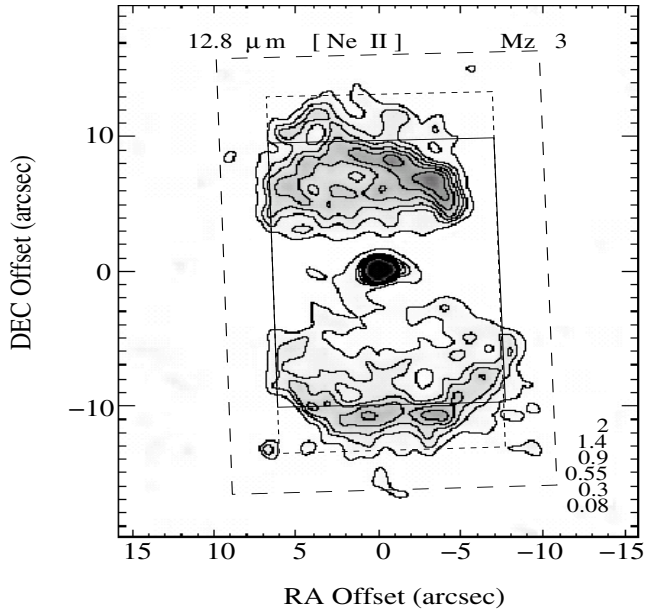


Fig. 1. Mz 3 in the [Ne II] 12.8 micron line with the ISO apertures superposed. The [Ne II] image is the deconvolved map of Smith & Gehrz (2005).

lobes which have an electron density of 10^4 cm^{-3} , while the lobes in the other two nebulae have a much lower density.

The nature of the central source is not completely understood. It contains the source of nebular ionization (the central star) but it also contains nebular emission. This is shown by several measurements. First, the spectrum of the central source contains emission lines. The visual spectrum through a very small diaphragm shows nebular forbidden lines ([O II], [O III], [N II] etc.) and emission lines of forbidden iron in several stages of ionization (Zhang & Liu 2002; Smith 2003). The infrared images clearly show [Ne II] strongly from the central source (Smith 2003; the VISIR observations, Lagage et al. 2004). Secondly the hydrogen lines are clearly seen in emission from the central source. Zhang & Liu (2002) measure $H\beta$ from the central source and Smith (2003) images Paschen α . The radio measurements show the central source quite clearly (Bains et al. 2004) in continuum emission. It is optically thick at the shortest wavelength measured (3.6 cm) and its size is less than $1''$. The VISIR observations show that the central nebula is diffraction limited, which means that its diameter probably is less than $0.4''$, and further it has an expansion velocity of about 50 to 70 km s^{-1} . The small size is related to the high density mentioned above, which was found from the forbidden iron lines. The age of the central nebula (depending on the distance) is probably less than 100 years and its mass is of order 3×10^{-4} solar masses.

In Fig. 1 an image of Mz3 is shown in the light of the [Ne II] line (taken from Smith & Gehrz 2005). The image is very similar to that shown in the light of Paschen α (Smith 2003). The ISO diaphragm is shown superimposed on the figure. More will be said presently over the ISO observations. We may already point out that one of the difficulties in interpreting the ISO data lies in the fact that the central source and the lobes

were measured together, but they must be analyzed separately because their densities are very different.

The purpose of this paper is primarily to determine the chemical abundances for this nebula which is of importance in discussing the evolution of the nebula. Secondly the analysis of the spectrum will yield information on the temperature of the exciting star. This goal is achieved first by analyzing the ISO spectroscopic data. Second, by applying state-of-the-art photoionization modeling, to attempt to reproduce the overall spectral energy distribution and the observed nebular emission line intensities in the visual and the infrared range. The abundances in this nebula have been determined earlier by Zhang & Liu (2002) and by Smith (2003), using only the visual spectrum.

The advantages of incorporating the ISO spectroscopy in our analysis have previously been discussed (e.g. see Pottasch & Beintema 1999; Pottasch et al. 2000, 2001; Bernard Salas et al. 2001), and can be summarized as follows.

The infrared lines originate from very low energy levels and thus give an abundance which is insensitive to the temperature in the nebula, and to possible temperature fluctuations. Furthermore, when a line originating from a high-lying energy level in the same ion is observed, it is possible to determine an effective (electron) temperature T_e at which the lines of that particular ion are formed. When T_e for many ions can be determined, it is possible to make a plot of T_e against ionization potential, which can be used to determine the T_e for ions for which only lines originating from a high energy level are observed. Use of an effective electron temperature takes into account the fact that ions are formed in different regions of the nebula. This way possible temperature fluctuations within the nebula can be taken into account.

Use of the ISO spectra have further advantages. One of them is that the number of observed ions used in the abundance analysis is approximately doubled, which removes the need for using large “ionization correction factors”, thus substantially lowering the uncertainty in the abundances derived for some elements.

A further advantage is that the extinction in the infrared is almost negligible, especially important because of the large extinction in Mz 3, and the fact that some of the extinction varies over the nebula.

A second method of improving the abundances is by using a nebular model to determine them. This has several advantages. First it provides a physical basis for the electron temperature determination. Secondly it permits abundance determinations for elements which are observed in only one, or a limited number of ionic stages, which could not be accurately determined without a model. A further advantage of modeling is that it provides physical information on the central star and other properties of the nebula. It thus allows one to take a comprehensive view of the nebula-star complex.

A disadvantage of modeling is that there are possibly more unknowns than observations and some assumptions must be made, especially concerning the geometry. In our case this is a special problem, since as can be seen in Fig. 1 the nebula cannot be assumed to be spherical, even as a first approach. This will be discussed in Sect. 4.

This paper is structured as follows. First the spectroscopic data are presented in Sect. 2. Section 3 discusses a simple approach to determine the chemical composition of Mz 3 and presents the resultant abundances. In Sect. 4 the model is presented and the assumptions made are discussed; this is followed by the abundance derivation. Sect. 5 compares the model spectrum with the observations. In Sect. 6 a comparison with earlier abundance determinations is made. The evolutionary state of the star-nebula system and the conclusions are given in Sects. 7 and 8.

2. The spectrum of Mz 3

In the following we present the available infrared and visual spectroscopic data used in our analysis. A compilation of the extinction corrected spectral line fluxes and identifications are given in Table 6.

2.1. The ISO observations

The ISO SWS observations were made with the SWS01 observing template. These measurements (TDT27300834) were centered at RA(2000) $16^{\text{h}}17^{\text{m}}13.6^{\text{s}}$ and Dec(2000) $-51^{\circ}59'06.4''$, which is very close to the center of the nebula. Data reduction was carried out using ISAP (ISO Spectral Analysis Package) version 2.1. The diaphragm used (shown in Fig. 1) was $14'' \times 20''$ below $12\mu\text{m}$, $14'' \times 27''$ between $12\mu\text{m}$ and $29\mu\text{m}$ and $20'' \times 33''$ above this wavelength. The entire nebula fit within the diaphragm in this last wavelength range, but it is possible that some nebular radiation was missed below $29\mu\text{m}$. This is a difficult problem because there may be an error of $1''$ or $2''$ in the position of the diaphragm and there may be a slight jitter during the observation which could effectively increase the diaphragm size by as much as $1''$. We shall therefore try to compare the observed fluxes with measurements taken with other diaphragms. The long wavelength observations were made with an LWS01 observation (TDT0842133) at essentially the same position, covering the wavelength range from $45\mu\text{m}$ to $200\mu\text{m}$. The diaphragm used had a diameter of $80''$ so the entire nebula was included. The intensity of the lines found in the spectrum is shown in Col. 3 of Table 1. The uncertainty of measurement of the stronger lines is less than 10%, while that of the weaker lines could be as large as 30%. The intensities of the LWS measurements agree reasonably well with those reported by Liu et al. (2001) shown in the last column. Also shown in the last column are the IRAS measurements (Pottasch et al. 1986).

2.1.1. IR flux from the lobes

As can be seen from Fig. 1 it is not clear whether or not the entire SWS emission of the lobes is included in the diaphragm. This is somewhat complicated by the fact that the precise position of the center is uncertain by one or two arcsecs and there may be a small jitter which effectively increases the diaphragm size by about the same amount. To study this further we compare the ISO measurements with measurements of Mz 3 which have been made with larger diaphragms. Two such

Table 1. ISO spectrum of Mz 3.

| Ident. | $\lambda(\mu\text{m})$ | Intensity | Comparison |
|----------|------------------------|-----------|------------|
| H I 5-4 | 4.051 | 22.0 | |
| [Ar II] | 6.985 | 76.9 | |
| H I 6-5 | 7.458 | 72.6 | |
| [Ar III] | 8.992 | 18.0 | |
| ?? | 10.350 | 9.8 | |
| [Co III] | 11.854 | 9.8: | |
| [Ne II] | 12.811 | 166.0 | 216.0 |
| [Ne III] | 15.560 | 11.4 | |
| [S III] | 18.709 | 124.0 | 80.: |
| [Fe III] | 22.915 | 26.7 | |
| [Fe II] | 25.974 | 5.5 | |
| [S III] | 33.475 | 72.2 | |
| [Si II] | 34.806 | 26.9 | |
| [O III] | 51.794 | 22.9 | 18. |
| [N III] | 57.305 | 34.7 | 35. |
| [O I] | 63.172 | 19.9 | 21.7 |
| [O III] | 88.391 | 6.79 | 7.0 |
| [N II] | 121.939 | 12.9 | 11.1 |
| [O I] | 145.561 | 1.61 | 0.75 |
| [C II] | 157.715 | 16.7 | |

Column 3 gives our measured values. The last column gives the IRAS measurements (Pottasch et al. 1986, and new unpublished data) below $20\mu\text{m}$, and the values of Liu et al. (2001) above $50\mu\text{m}$. All intensities are in units of $10^{-12} \text{ erg cm}^{-2} \text{ s}^{-1}$. The “:” on some line intensities indicates uncertain values.

measurements are available: the IRAS measurements and the radio frequency measurements.

The IRAS measurements consist of the survey results which made measurements with a large bandwidth and the low resolution spectrograph (LRS) measurements. The survey results are 88.8 Jy in the $12\mu\text{m}$ band (between 8 and $15\mu\text{m}$) and 343 Jy in the $25\mu\text{m}$ band (between 18 and $30\mu\text{m}$). These measurements are plotted on a “quick look” ISO SWS spectrum in Fig. 2 where it can be seen that the IRAS measurements are higher. A more detailed analysis gives the same result: the IRAS results are about 25% to 35% higher than the ISO results. This also agrees with the jump in the spectrum above $30\mu\text{m}$ by about this amount which was measured with the larger aperture including the entire nebula.

The LRS spectrum included the $12.8\mu\text{m}$ line of [Ne II]. A recent unpublished reduction yields an intensity of $2.16 \times 10^{-10} \text{ erg cm}^{-2} \text{ s}^{-1}$ for this line, which is somewhat higher than an earlier reduction (Pottasch et al. 1986). It is also about 30% higher than the ISO SWS measurement shown in Table 1. The error on the IRAS measurement is probably also about 30%, so that the only conclusion which can be made is that it is consistent with 30% of the flux being missed in the ISO diaphragm.

The radio continuum flux density, which can be measured separately for the central source and the lobes, can be used to derive the intrinsic $\text{H}\beta$ flux from each of these entities (Bains et al. 2004). These are related as follows. From the measured 6 cm flux density an intrinsic $\text{H}\beta$ flux is derived. By using the theoretical hydrogen line intensity ratios (Hummer & Storey 1987) for an electron temperature of 7500 K (see below) the intrinsic values of Brackett α and Pfund α can be found and

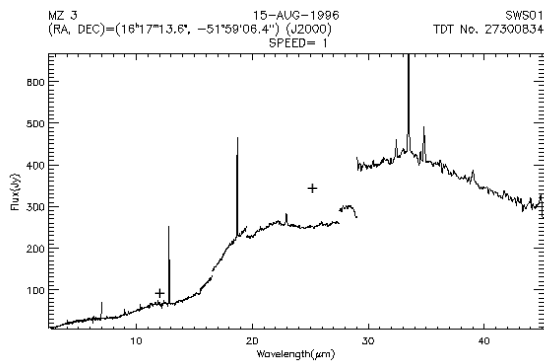


Fig. 2. The ISO spectrum with 12 and 25 micron IRAS fluxes overplotted as crosses.

compared to the ISO measurements of these lines in Table 1. There is one difficulty however: the radio emission from the central source is optically deep at 6 cm, and possibly at 2 cm as well. To correct for this we assume that the intrinsic radio emission from the central source is the same percentage of the total radio emission as the measured $H\beta$ from the central source is of the total measured $H\beta$ emission (22%, see below). This leads to a total intrinsic radio flux density of 770 mJy at 6 cm (600 mJy from the lobes and 170 mJy from the central source). This would predict a total $H\beta$ flux of 2.86×10^{-10} erg cm $^{-2}$ s $^{-1}$, a Br α flux of 2.48×10^{-11} erg cm $^{-2}$ s $^{-1}$ and a Pf α flux of 7.94×10^{-12} erg cm $^{-2}$ s $^{-1}$. Comparing these expectations to the measured values in Table 1 it appears that we are missing only 12 to 13% of the expected emission.

Because of the uncertainties involved in these estimates we use an average of the two methods and assume that we are missing between 10% and 30% of the total emission below 30 μ m. Above this wavelength no emission is being missed.

2.1.2. IR flux from the central source

There are several infrared measurements of the central source. Aitken & Roche (1982) have measured the spectrum between 8 μ m and 13 μ m with a 5.3'' diameter diaphragm which allows only negligible lobe emission. Smith & Gehrz (2005) have made narrow band filter measurements using a 4'' diaphragm. They obtain practically identical results. For the 12.8 μ m line of [Ne II] they find an intensity of 2.88×10^{-11} erg cm $^{-2}$ s $^{-1}$. This is about 17% of the emission found by ISO for the sum of emission from the lobes and the central source. This agrees with the result of the previous section that between 10% and 30% of the hydrogen emission comes from the central source. While the spectrum of the central source and the lobes will not be exactly the same, it is likely that an assumption that 20% of all measured line intensity comes from the central source will not be substantially in error.

2.1.3. Resultant IR lobe emission

To obtain the abundances from a given ion, the intensity of a line of that ion with respect to a hydrogen line is required. For the ISO lines measured with the SWS, the intensity from

the lobes and the central source are measured together and it is necessary to correct for the intensity of the central source. As discussed in Sect.2.3, about 22% of the hydrogen emission comes from the central source. In Sect.2.1.2 it was found that about 17% of the [NeII] 12.8 μ m emission comes from the central source. Thus to a first approximation the ratio of the [NeII] emission line to a hydrogen line is the same in the lobe as in the total emission as given in Table 1. Whether or not this is true for the other SWS lines is not certain because the spectrum of the central source and the lobes is not necessarily the same. However the level of ionization of the other SWS lines is similar and it would be surprising if large differences occur. Zhang & Liu (2002) have measured the optical spectra in both regions and do not find a strongly differing ionization state in the two regions. Even if, for example, the [ArIII] line were only half as strong in the central source, the assumption that the spectra are the same would introduce only a 10% error.

Above 30 μ m the diaphragm was large enough to measure the total emission and here also the radiation coming from the central source should be subtracted. Thus lobe intensities above 30 μ m are 20% lower than given in Table 1. The intensity ratio is obtained by dividing this by the value of the $H\beta$ emission coming from the lobe, which is 2.86×10^{-10} erg cm $^{-2}$ s $^{-1}$; this value is corrected for extinction since it is derived from the radio flux density. This affects only the N $^+$, N $^{++}$ and O $^{++}$ abundances. But because of the low state of ionization, the nitrogen and oxygen abundances depend primarily on the N $^+$ and O $^+$ abundances. The N $^+$ abundance obtained from the ISO far infrared line can be checked using the λ 6584 \AA in the visual; these two lines yield the same result, as shown in Table 4. The oxygen abundance is dependent on the visual line at λ 3727 \AA .

Very early in the analysis we tried to make a model of the core in order to predict more precisely the spectrum of the central source. This was unsuccessful, probably because the nature of the core is not well enough known.

2.2. The visual spectrum

The optical spectrum of Mz 3 has been measured on two occasions in the past five years. Both Zhang & Liu (2002) and Smith (2003) have measured the spectrum in similar ways. Both use a long slit about 2'' wide. The slit is oriented north-south in both cases and goes through the central nebula. Both are able to obtain a spectrum of the central nebula and the lobes on the north and the south side. They find that the spectra are the same in the north as in the south. The spectral resolutions used are quite similar and vary somewhat with the spectral region. The spectrum of Smith extends further to the red so that some of the Paschen lines are measured. Both spectra appear to come from the same regions of the lobes but they differ somewhat from each other. The measured intensities of both authors are similar on the red side of $H\beta$. They differ by approximately a factor of 2 on the blue side. They therefore give different reddening corrections, using the same method of trying to reproduce the expected theoretical hydrogen line intensities using the theory of Hummer & Storey (1987). After reddening correction the intensities relative to $H\beta$ agree better with one another.

The $H\alpha$ intensity of Smith is rather high but his Paschen line intensities agree well with theoretical predictions (except for Pa8 which is near the edge of his spectrum). The critical OII lines at $\lambda 3727 \text{ \AA}$ now agree to within 25%. We shall use the average value of the two authors after they have corrected for reddening. The [SIII] line at $\lambda 9531 \text{ \AA}$ was taken only from Smith. The averaged fluxes are listed in Table 6.

2.3. Extinction

There are several methods for estimating the extinction towards planetary nebulae. We have already mentioned the comparison of observed and theoretical Balmer decrement and the uncertainties which can result. Perhaps the most reliable method is a comparison of radio emission with $H\beta$ flux. As discussed in Sect. 2.1.1 the $\log H\beta$ flux found from the radio measurement of the lobes is -9.55 . The measured $\log H\beta$ flux from the entire nebula is -11.09 (Webster 1969) while the $\log H\beta$ flux from the central source is -11.75 . Thus $\log H\beta = -11.20$ originates from the lobes. Comparing this with the predicted $H\beta$ we obtain $c = 1.65$ or $E_{B-V} = 1.13$. This is in rough agreement with the much more uncertain values obtained from the Balmer (and Paschen) decrement: Smith (2003) finds $c = 1.5$ and Zhang & Liu (2002) give $c = 2.0$ for the lobes and a somewhat higher value for the central region. This value, $c = 1.65$ has been adopted in the remainder of this paper, together with the extinction curves of Seaton (1979) and Fluks et al. (1994). It is actually not needed for the visual spectrum as discussed above, nor is it needed for the determination of the $H\beta$ flux which is found from the radio measurements. It is an unusually high extinction so that even the far infrared fluxes are slightly affected. We have corrected these values (the corrected values are given in Table 6) but the correction is small, usually less than 10%.

3. Chemical composition of Mz 3 from the simplified analysis

The method of analysis is the same as used in the papers cited in the introduction. First the electron density and the temperature as function of the ionization potential are determined. Then the ionic abundances are determined, using the density and the temperature appropriate for the ion under consideration, together with Eq. (1). Then the element abundances are found for those elements for which a sufficient number of ionic abundances have been derived.

3.1. Electron density

The ions used to determine N_e are listed in the first column of Table 2. The ionization potential required to reach that ionization stage, and the wavelengths of the lines used, are given in Cols. 2 and 3 of the table. Note that the wavelength units are \AA when 4 ciphers are given and microns when 3 ciphers are shown. The observed ratio of the lines is given in the fourth column; the corresponding N_e is given in the fifth column. The temperature used is discussed in the following section, but is unimportant since these line ratios are essentially determined by the density. The atomic parameters used are the same as in

Table 2. Electron density indicators in Mz 3.

| Ion | Ioniz. Pot. (eV) | Lines used | Observed ratio | N_e (cm^{-3}) |
|----------|------------------|------------|----------------|----------------------------|
| [S II] | 10.4 | 6731/6716 | 1.83 | 5000 |
| [O II] | 13.6 | 3626/3729 | 1.90 | 3500 |
| [S III] | 23.3 | 33.5/18.7 | 0.437 | 3300 |
| [Cl III] | 23.8 | 5538/5518 | 1.80 | 10 000 |
| [O III] | 35.1 | 51.8/88.4 | 3.37 | 2000 |

Table 3. Electron temperature indicators in Mz 3.

| Ion | Ioniz. Pot. (eV) | Lines used | Observed ratio | T_e (K) |
|----------|------------------|------------|----------------|-----------|
| [N II] | 14.5 | 5755/6584 | 0.0055 | 6700 |
| [N II] | 14.5 | 6584/122 | 128. | 6900 |
| [S III] | 23.3 | 6312/18.7 | 0.0175 | 7900 |
| [Ar III] | 27.8 | 7136/8.99 | 0.83 | 8700 |
| [O III] | 35.1 | 4363/5007 | 0.0175 | 13 700 |
| [O III] | 35.1 | 5007/51.8 | 3.3 | 7700 |
| [Ne III] | 41.0 | 3868/15.5 | 0.84 | 10 800 |

the earlier papers cited above. The only exception to this is the case of [O II] for which the values recently recommended by Wang et al. (2004) have been used.

The electron density appears to be about 4000 cm^{-3} . There is no indication that the electron density varies with ionization potential in a systematic way, although a limited number of values are determined.

3.2. Electron temperature

A number of ions have lines originating from energy levels far enough apart that their ratio is sensitive to the electron temperature. These are listed in Table 3, which is arranged similarly to the previous table. The electron temperature is found to increase as a function of ionization potential. There is some scatter. A value of $N_e = 4000 \text{ cm}^{-3}$ has been used in the computations, but the temperature is in general not sensitive to the electron density.

3.3. Ionic and element abundances

The ionic abundances have been determined using the following equation:

$$\frac{N_{\text{ion}}}{N_p} = \frac{I_{\text{ion}}}{I_{H\beta}} N_e \frac{\lambda_{\text{ul}}}{\lambda_{H\beta}} \frac{\alpha_{H\beta}}{A_{\text{ul}}} \left(\frac{N_u}{N_{\text{ion}}} \right)^{-1} \quad (1)$$

where $I_{\text{ion}}/I_{H\beta}$ is the measured intensity of the ionic line compared to $H\beta$, N_p is the density of ionized hydrogen, λ_{ul} is the wavelength of this line, $\lambda_{H\beta}$ is the wavelength of $H\beta$, $\alpha_{H\beta}$ is the effective recombination coefficient for $H\beta$, A_{ul} is the Einstein spontaneous transition rate for the line, and N_u/N_{ion} is the ratio of the population of the level from which the line originates to the total population of the ion. This ratio has been determined using a five level atom.

The results are given in Table 4, where the first column lists the ion concerned, and the second column the line used for the abundance determination. The third column gives the intensity of the line used relative to $H\beta = 100$. The fourth column gives the electron temperature used, which is a function of the ionization potential and is found or interpolated from Table 3. The ionic abundances, are in the fifth column, while the sixth column gives the Ionization Correction Factor (ICF). This has been determined empirically. Notice that the ICF is unity for carbon, nitrogen, oxygen, neon and argon because all important stages of ionization have been observed. The ICFs for the other elements have been determined by comparing the observed ionization stages as a function of ionization potential with those elements where all important ionization stages are present. Only one stage of ionization has been observed in silicon and chlorine for which only a model approach can give a trustworthy result. No helium abundance has been given because no reliable correction for neutral helium can be made without a model. The carbon abundance is an upper limit because it is probable that the C^+ line at $\lambda 157.6 \mu\text{m}$ originates in the surrounding interstellar medium, at least partially. No background spectrum is available because of the presence of HII emission regions in the neighborhood (see the discussion of Liu et al. 2001). The C^{++} abundance is derived from the recombination line $\lambda 4267 \text{ \AA}$; while this give a reasonable ratio for the two carbon ions, it sometimes overestimates the C^{++} abundance.

The ionized helium abundance has been derived using the theoretical work of Benjamin et al. (1999). For recombination of singly ionized helium, most weight is given to the $\lambda 5875 \text{ \AA}$ line, because the theoretical determination of this line is the most reliable.

The final abundances are shown in the second column of Table 7. Of the eight elements for which an abundance is given, six can be determined using only ISO measurements. These are nitrogen, neon, sulfur, argon, iron and silicon. These abundances are essentially independent of electron temperature and not very dependent on electron density for the density range expected. The abundances in Mz 3 differ in general from solar abundances. The oxygen abundance is about half solar, while nitrogen is about a factor of five higher. Neon, argon, silicon, sulfur and chlorine are within a factor of two of solar. Iron is about a factor of four lower than solar but it is an order of magnitude higher than in other planetary nebulae. We shall discuss these abundances in more detail presently.

4. Model

In order to obtain as nearly a correct model as possible, the star as well as the nebula must be considered. Let us first consider the star. There are several ways to obtain a reasonable estimate of the stellar temperature.

Modeling the nebula-star complex will allow characterizing not only the central star's temperature but other stellar parameters as well (i.e., $\log g$ and luminosity). It can determine distance and other nebular properties, especially the composition, including the composition of elements which are represented by a single stage of ionization, which cannot be determined by the simplified analysis above. This method can take

Table 4. Ionic concentrations and chemical abundances in Mz 3. Wavelength in Angstrom for all values of λ above 1000, otherwise in μm .

| Ion | λ | I | T | $N_{\text{ion}}/N_{\text{p}}$ | ICF | $N_{\text{el.}}/N_{\text{p}}$ |
|------------------|-----------|--------|--------|-------------------------------|-----|-------------------------------|
| He ⁺ | 5875 | 12.0 | 9 000 | 0.080 | | |
| C ⁺ | 157.6 | ≤4.67. | 7 000 | ≤1.19(-3) | | |
| C ⁺⁺ | 4267 | 0.377 | 10 000 | 4.2(-4) | 1 | ≤1.6(-3) |
| N ⁺ | 6584 | 465. | 7 000 | 2.46(-4) | | |
| N ⁺ | 122. | 3.61 | 7 000 | 2.67(-4) | | |
| N ⁺⁺ | 57.3 | 9.7 | 12 000 | 4.97(-5) | 1 | 3.0(-4) |
| O ⁺ | 3726 | 42. | 7 000 | 2.06(-4) | | |
| O ⁺⁺ | 5007 | 21.5 | 12 000 | 6. (-6) | | |
| O ⁺⁺ | 51.8 | 6.4 | 12 000 | 2.25(-5) | 1 | 2.3(-4) |
| Ne ⁺ | 12.8 | 64. | 8 000 | 1.15(-4) | | |
| Ne ⁺⁺ | 15.5 | 4.2. | 12 000 | 4.18(-6) | | |
| Ne ⁺⁺ | 3869 | 1.4 | 12 000 | 1.7(-6) | 1 | 1.2(-4) |
| S ⁺ | 6731 | 13.5 | 7 000 | 2.04(-6) | | |
| S ⁺⁺ | 6312 | 0.84 | 8 000 | 5.3(-6) | | |
| S ⁺⁺ | 18.7 | 48.1 | 8 000 | 5.82(-6) | | |
| S ⁺⁺ | 33.5 | 21.0 | 8 000 | 7.09(-6) | 1.2 | 1.0(-5) |
| Ar ⁺ | 6.99 | 28.5 | 7 500 | 4.02(-6) | | |
| Ar ⁺⁺ | 7136 | 7.1 | 11 000 | 7.0(-7) | | |
| Ar ⁺⁺ | 8.99 | 8.24 | 11 000 | 1.03(-6) | 1 | 5.0(-6) |
| Cl ⁺⁺ | 5538 | 0.45 | 8 000 | 1.3(-7) | 1.4 | 1.8(-7) |
| Fe ⁺ | 25.9 | 2.3 | 7 000 | 6.27(-7) | | |
| Fe ⁺³ | 22.9 | 10.8 | 8 000 | 4.52(-6) | 1.5 | 7.8(-6) |
| Si ⁺ | 34.8 | 8.33 | 7 000 | 5.8(-6) | 3: | 1.8(-5) |

Intensities (I) given with respect to $H\beta = 100$. The colon “:” indicates an uncertain correction for the missing ionization stages.

into account the presence of dust and molecules in the nebular material and thus is very comprehensive in approach. While the line ratio method is simple and fast, the ICFs rest on uncertain physics. To this end, modeling serves as an effective means and the whole set of parameters are determined in an unified way, assuring self consistency. Finally, this way one gets a good physical insight about the PN, the method and the observations.

It is with this in mind that we have constructed a photoionization model for Mz 3 with the code Cloudy, using the latest version C96.01 (Ferland et al. 1998).

4.1. Open geometry

Mz 3 presents a complex geometry; to a good approximation it is a bipolar nebula with the two lobes presenting a dome-like shape surrounded by plumes of gas. An additional complication is that the density does not seem to be uniform within these lobes. Here we only model one lobe (northern part) of the nebula by way of invoking “an open geometric model”. This introduces a “covering factor” $\Omega/4\pi$. “Covering factor” is the fraction of 4π steradians covered by the gas, as viewed from the central source of ionizing radiation. For example a spherical shell will have a covering factor of a full 4π steradians. In a spherical shell, the inward bound diffuse radiation can go

over to the far side of the central source and can ionize/heat the material present there. In the case of an “open geometry”, the “covering factor” being smaller than 4π steradians, the radiation emitted from the illuminated face of the lobe towards the central source, escapes from the system. A good analogy can be the broad-line region of an AGN or the filaments within the Crab Nebula. The reader is referred to Cloudy’s user manual for more details. To model one lobe of Mz 3, since we can not measure the “covering factor” from the available images (which give only 2-D information), we need to try various reasonable estimates till we get the best match with observed spectra. To handle the variation in density we invoke the conventional “filling factor”.

4.2. Other assumptions in the model

From the available literature on Mz 3, we find that this PN is quite complex in many respects. Apart from the aforementioned factors like geometry and density fluctuations, the nebula is also known to emit X-rays (Kastner et al. 2003). The X-ray luminosity is very small and so we neglect it in the overall energetics. The central star is thought to be a binary. Also high resolution spectroscopy (Redman et al. 2000; Guerrero et al. 2004; and Santander- Garcia et al. 2004), reveal that the gas is flowing along the polar axis at high velocities of $300\text{--}500\text{ km s}^{-1}$. We have to look at the finer aspects of this: the line photons from one lobe emitted towards the other lobe would get doppler shifted and would not be absorbed by the other lobe, whereas the continuum photons could be absorbed. Here we are modeling a single static lobe in steady state and neglect the interaction with any radiation from the other lobe. In early simulations, we tried to incorporate dual central source (two stars, one hot and one cool), but later on tried only a single star represented by model atmospheres (Atlas) from Kurucz (1991). It was found that the addition of a cool star did not make any significant difference. We have considered only the gas phase abundances of the various elements seen in the spectra (Table 6), though it is known that dust grains are present (Smith & Gehrz 2005). For a bipolar nebula, Mz 3 does not show any significant molecular emission. The angular extent of the lobe to be modelled was calculated as 16 arcsec from the distribution of emission along the slit as shown in Fig. 6 of Smith (2003). Almost all the lobe emission (in lines) is within this extent. When comparing the model spectra with observed spectra, we had practical difficulties. The two recently published CCD spectra by Zhang & Liu (2002) and by Smith (2003), differ in observed fluxes of various lines as mentioned earlier in Sect. 2.2. We have used an average value, although we could have given both values to indicate the range observed. The ISO spectrum was observed over the entire nebula (see Fig. 1), and we assumed that the ratio of line intensity to $H\beta$ intensity is the same in both lobes. The $H\beta$ flux (see earlier) appropriate for the entire nebula was derived as $2.86 \times 10^{-10}\text{ ergs cm}^{-2}\text{ s}^{-1}$. We note that the northern lobe emits slightly more radiation and assumed that this is around 60% of the total ($1.72 \times 10^{-10}\text{ ergs cm}^{-2}\text{ s}^{-1}$). This 60:40 ratio is approximately the ratio of the radio emission of these lobes.

Table 5. Parameters representing the best-fit model.

| Parameter | Value | | | |
|-------------------------|--|--|--|--|
| <i>Ionizing source</i> | | | | |
| <i>Model atmosphere</i> | Atlas | | | |
| T_{eff} | 39 300 K | | | |
| Log g | 5.0 | | | |
| Luminosity | 9100 L_{\odot} | | | |
| <i>Nebular lobe</i> | | | | |
| Const. density | $N_{\text{H}} = 4.45 \times 10^3\text{ cm}^{-3}$ | | | |
| Abundance | H He C N | | | |
| | 12.000 11.301 8.420 8.574 | | | |
| | O Ne Si S | | | |
| | 8.340 8.041 7.300 7.000 | | | |
| | Cl Ar K Cr | | | |
| | 5.376 6.431 5.079 -8.0 | | | |
| | Mn Fe Co Ni | | | |
| | -8.0 7.000 -8.0 4.255 | | | |
| Size | 16" (extent) | | | |
| Distance | 1.30 kpc | | | |
| Covering factor | 0.28 | | | |
| inner radius | 2.512e15 cm ($\sim 0.00081\text{ pc}$) | | | |
| outer radius | 3.112e17 cm ($\sim 0.10\text{ pc}$) | | | |
| Filling factor | 0.28 | | | |

4.3. Results

The general method of application of the code Cloudy to model Mz 3 is the same as in Surendiranath et al. (2004) and Pottasch & Surendiranath (2005); we ran a number of models and each time the output was carefully scrutinized before running the next model with changed input parameters. We tried to match the observed spectral fluxes of about 50 lines and we relied on physical intuition rather than any of the optimization techniques provided in Cloudy. In spite of the many uncertainties and complexities involved, our final model is considered to be moderately successful.

Table 5 gives the input parameters of the best matched model, and the corresponding output spectral fluxes are compared to the observed ones in Table 6.

5. Discussion

The best-fit model input parameters are our final values for the characteristics of the polar lobe of the PN and its ionizing source.

5.1. Nebular density and temperature

The electron density and temperature as computed by our model is plotted in Fig. 3 against nebular depth, i.e., the radial distance calculated from the inner surface of the lobe. The mean density of $\sim 5000\text{ cm}^{-3}$ is reasonable compared to the values in Table 2 which were derived from individual line ratios. We have used a filling factor to take care of the density fluctuations and the available HST image (www.spacetelescope.org/images/html/heic0101a.html) indicates quite complex variations. The agreement with the determinations of

Table 6. The emission line fluxes ($H\beta = 100$).

| Label | line | Model flux | Obsd. flux (dereddened) | Label | line | Model flux | Obsd. flux (dereddened) |
|----------|--------|------------|----------------------------|-------|---------|------------|----------------------------|
| TOTL | 4861 A | 100.00 | 100.00 | N 2 | 6584 A | 458.66 | 466.00 |
| O II | 3726 A | 40.30 | 41.80 | He 1 | 6678 A | 3.28 | 3.65 |
| O II | 3729 A | 14.89 | 22.30 | S II | 6716 A | 6.31 | 7.25 |
| Ne 3 | 3869 A | 1.40 | 1.25 | S II | 6731 A | 11.39 | 12.90 |
| S 2 | 4074 A | 3.20 | 4.02 | He 1 | 7065 A | 6.41 | 4.14 |
| C 2 | 4267 A | 0.08 | 0.35 | Ar 3 | 7135 A | 6.84 | 6.88 |
| H 1 | 4340 A | 46.70 | 47.50 | Fe 2 | 7155 A | 0.13 | 0.43 |
| TOTL(O3) | 4363 A | 0.17 | 0.36 | O II | 7323 A | 1.77 | 1.94 |
| He 1 | 4471 A | 4.10 | 3.98 | O II | 7332 A | 1.35 | 1.56 |
| Fe 3 | 4658 A | 2.61 | 2.75 | S 3 | 9532 A | 72.19 | 73.20 |
| Fe 2 | 4815 A | 0.05 | 0.78 | H 1 | 4.051 m | 9.20 | 8.54 |
| Fe 2 | 4890 A | 0.03 | 0.40 | Ar 2 | 6.980 m | 16.53 | 28.50 |
| Fe 2 | 4905 A | 0.01 | 0.39 | Ar 3 | 9.000 m | 8.35 | 8.24 |
| O 3 | 4959 A | 14.46 | 6.49 | Ne 2 | 12.81 m | 60.39 | 64.00 |
| O 3 | 5007 A | 43.52 | 21.20 | Ne 3 | 15.55 m | 2.88 | 4.19 |
| Fe 2 | 5159 A | 0.15 | 0.40 | S 3 | 18.67 m | 55.93 | 48.10 |
| N 1 | 5200 A | 0.37 | 0.98 | Fe 2 | 25.99 m | 1.13 | 2.29 |
| Fe 3 | 5270 A | 1.49 | 1.11 | S 3 | 33.47 m | 14.59 | 21.00 |
| Cl 3 | 5518 A | 0.35 | 0.26 | O 3 | 51.80 m | 5.17 | 6.41 |
| Cl 3 | 5538 A | 0.46 | 0.48 | N 3 | 57.21 m | 12.24 | 9.71 |
| N 2 | 5755 A | 2.87 | 2.53 | O 1 | 63.17 m | 0.06 | 5.57 |
| He 1 | 5876 A | 12.16 | 11.50 | O 3 | 88.33 m | 0.82 | 1.90 |
| O 1 | 6300 A | 0.15 | 0.87 | N 2 | 121.7 m | 2.32 | 3.61 |
| S 3 | 6312 A | 0.96 | 0.84 | O 1 | 145.5 m | 0.003 | 0.45 |
| O 1 | 6363 A | 0.05 | 0.38 | C 2 | 157.6 m | 0.45 | 4.67 |
| N 2 | 6548 A | 155.42 | 156.00 | | | | |

Absolute $H\beta$ flux (n.lobe) Model: 1.68×10^{-10} ergs cm^{-2} s^{-1} . Obsn: 1.72×10^{-10} ergs cm^{-2} s^{-1} .

Notes: “A” in col. “Line” signifies Angstrom; “m” signifies μm . In Col. “Label”, we have followed the notation used by Cloudy for atoms and ions; this will make identifying a line in Cloudy’s huge line list easy. Neutral state is indicated by “1” and singly ionized state by “2” etc., “TOTL” typically means the sum of all the lines in the doublet/multiplet; or it could mean sum of all processes: recombination, collisional excitation, and charge transfer. Some elements are represented by usual notation as per Cloudy.

Zhang & Liu (2002) and Smith (2003) is very good. The mean electron temperature from our model of ~ 8000 K is higher by about 1000 K as compared to the determinations of both these authors. This has to do with the uncertainty in the energy distribution of the ionizing source (see Sects. 5.2 and 5.3 below).

5.2. Comparison of model spectrum with observation

As mentioned earlier we have attempted to obtain a good match for about 50 observed lines and these are shown in Table 6. Cloudy computes by default the fluxes of continuum at various wavelengths and a very large of number emission lines (nearly 2000) in its output spectrum. The overall match seems to be all right except for some peculiarities. The diagnostic lines of O II, N II, S II and Cl III came out clean in the matching game. The helium lines also did well. If you consider S III, you find that it is represented by many lines over a range of wavelengths, and the model produces correct flux in the optical and far-red

regions while IR lines are deviant. The reason could be either the integration of the optical with ISO spectra is not seamless or the fine structure lines are affected in a way we do not understand. The optical spectrum was observed with a long slit while the ISO observations were through apertures of varying sizes (see Fig. 1). As discussed earlier, this factor and the extent of contribution of the central region (core) to the lobe spectrum were taken care of, for the IR lines. O III lines also behave in a peculiar way. Fe III lines did fine while Fe II lines failed. One problem that we guess is that the density inhomogeneity is so great that the mechanism of filling factor could not handle it. There could also be a problem with the inputted model atmosphere fluxes for the central source, since we have no way of constraining them with observations (see next subsection). For carbon, increasing the model abundance increases the flux in C II lines but upsets the good match achieved in many other lines, more so in N II and O II. This is why the carbon abundance determined by the line ratio method (Table 4) must be

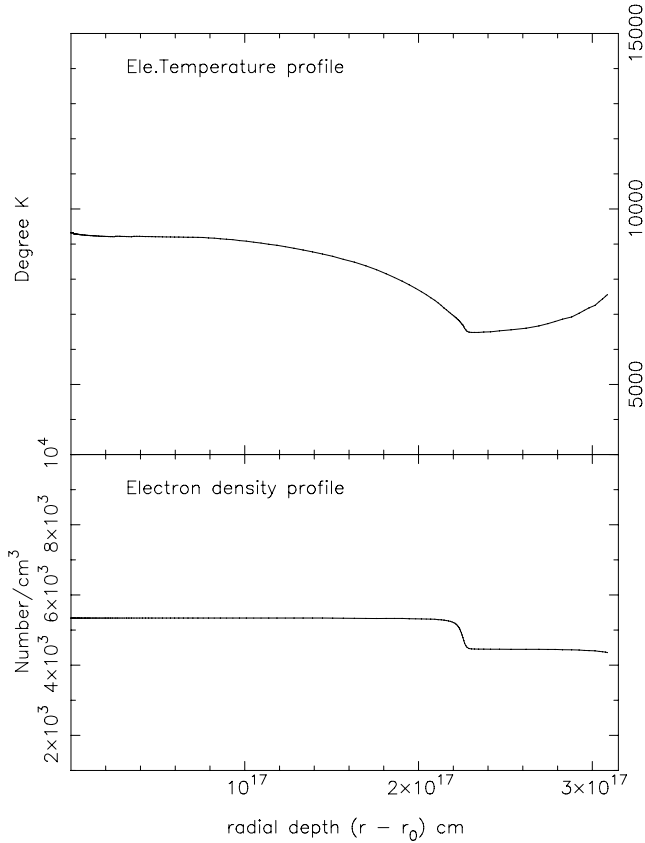


Fig. 3. T_e and N_e across the nebula.

too high. The model abundance of carbon given in Tables 5 and 7 should only be considered as an upper limit. Basically we sought an underlying simplicity behind the apparent complexity and we feel that our open geometric model for the polar wing of Mz 3 is a moderate success, when viewed in the backdrop of all the uncertainties and unknowns.

5.3. Central star

The central star of Mz 3 is not resolved. At the center of the PN there is a sub-arcsecond high density ($N_e \sim 10^6 \text{ cm}^{-3}$) nebular core (see Zhang & Liu 2002) which is not modelled here. This region also hosts a dust torus. The ionizing source whose characteristics we have derived from our model of the lobe does not describe the central star since the energetics involved in ionizing the high density core is not known. What is given in Table 5 for the ionizing source pertains to the energy coming out at the exit point of this core. The difficulty we mentioned in the previous subsection about the use of model atmosphere flux refers to this aspect. A more realistic representation would involve the modification of the model atmosphere flux distribution over select wavelength regions as part of the modeling methodology or including core modeling too, but we have not done either. Figure 4 shows the incident and the transmitted energy in the model. The absorption below 912 Å is more or less complete except between 500 Å and 650 Å. Therefore, we predict that the central star ought to be hotter than the T_{eff} listed in Table 5 or more luminous than what we computed or both,

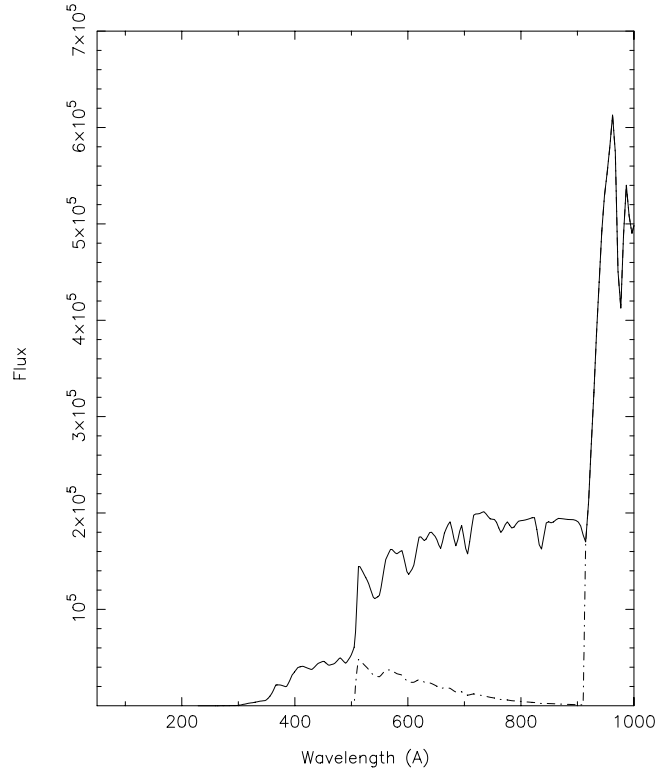


Fig. 4. Stellar ionizing radiation – Incident (continuous line) and transmitted (broken line).

Table 7. Abundances in Mz 3.

| Element | Present ICF | Present model | Zhang Liu | Smith | NGC 6537 | Solar |
|---------|--------------|---------------|-----------|-------|----------|-------|
| He | ≥ 0.080 | 0.20 | 0.086 | 0.20 | 0.149 | 0.085 |
| C(-4) | ≤ 16 . | ≤ 2.63 | | | 1.75 | 2.5 |
| N(-4) | 3.0 | 3.75 | 2.4 | 4.7 | 4.5 | 0.61 |
| O(-4) | 2.3 | 2.18 | 3.2 | 4.4 | 1.85 | 4.6 |
| Ne(-4) | 1.2 | 1.10 | 0.44 | 0.60 | 1.7 | 1.2 |
| Si(-5) | 2.0 | 2.0 | | 0.46 | | 3.3 |
| S(-5) | 1.0 | 1.0 | 1.4 | 1.2 | 1.1 | 1.4 |
| Cl(-7) | 1.8 | 2.38 | 1.9 | | 2.4 | 3.5 |
| Ar(-6) | 5.0 | 2.70 | 14. | 4.8 | 4.1 | 2.5 |
| Fe(-6) | 7.8 | 10.0 | 12.6 | | | 28. |

The abundances listed “Zhang & Liu” are from Zhang & Liu (2002), those listed “Smith” from Smith (2003), NGC 6537 from Pottasch et al. (2000) and Solar abundances are from Apslund et al. (2005) except for Ne and Ar.

since the core region would consume some energy in getting ionized, apart from energy consumption by dust grains as well.

6. Nebular abundances

The abundances derived by the two methods are compared in Table 7.

Two earlier abundance determinations are also listed in Table 7. Those of Zhang & Liu (2002) are based only on the visual spectrum so that no carbon abundance can be determined. Only one nitrogen line was observed (NII). Smith (2003)

include part of the near infrared spectrum but the emphasis is on the visual lines in deriving the abundances.

We are capable of obtaining more accurate electron temperatures thanks to the inclusion of the far infrared observations. Eight temperature determinations are given in Table 4 over a wide range of ionization potentials, while earlier abundance analyzes had only two temperature determinations. Our carbon abundance may only be an upper limit however.

7. Evolutionary state

The helium abundance can only be found by correcting for the presence of neutral helium in the nebula. We have done this by making use of a model and we obtain the same result as Smith (2003). This is a very high helium abundance, comparable to that seen in the bipolar planetary nebulae NGC 6302 (Pottasch et al. 1999) and NGC 6537, and the rather amorphous PN He2-111 (Pottasch et al. 2000). Just as Mz 3 all these nebulae are located close to the galactic plane and have high extinction. Furthermore they all have abundances very similar to Mz 3. As example, the abundances in NGC 6537 are shown in the sixth column of Table 7. In all these nebula the helium must have been produced in the course of the evolution of the central stars of these objects. The large amount of nitrogen found in Mz 3 is the same as found in these other nebulae. All have nitrogen to oxygen ratios of about unity and an oxygen abundance of about one half solar. A consequence of this is that the rather high nitrogen and helium abundance was probably produced by hot bottom burning. For this to occur the initial stellar mass should be at least 4 solar masses. Since the three nebulae cited all have carbon to oxygen ratios between 0.5 and 1 strengthens our feeling that the carbon abundance given in Table 7 for Mz 3 is only an upper limit.

8. Conclusion

We have presented the ISO far infrared spectrum of Mz 3. From the ISO spectrum alone we have been able to find the abundance of six elements in the inner lobes of this nebula. These are nitrogen, neon and argon for which all important stages of ionization have been measured by ISO, and sulfur, iron and silicon whose abundances improved with the use of a model. Including the visual spectrum this has enabled us to derive nebular abundances of 9 elements and a lower limit to the helium abundance. In addition, a simplified nebular model (electron temperature and density) has been found. These abundances have been improved by using a more elaborate photoionization modeling in an open geometric configuration. The model indicates that a rather large amount of neutral helium exists and that the helium abundance is probably twice as large as in the sun. This last result confirms the helium abundance previously found (Smith 2003).

The results are given in Tables 4 and 5 and summarized in Table 7. A comparison with earlier work is also given in the last table. The abundances found are also very similar to those found in other bilobal planetary nebulae showing high helium and nitrogen abundances.

The difficulty in deriving the details of the central star's ionizing energy distribution has been discussed. Lower limits to the T_{eff} and luminosity are obtained. Taken together, the nebular abundances and the probable stellar parameters suggest that Mz 3 is probably descended from a star of at least 4 solar masses.

Acknowledgements. We would like to acknowledge the use of SIMBAD and ADS for this work. RS thanks Baba Antony Varghese for help with the graphics and data recovery after a system crash; J.S. Nathan helped by lending a "linux box" in time.

References

- Acker, A., Ochsenbein, F., Stenholm, B., et al. 1992, *Strasb.-ESO Catalogue*
- Aitken, D.K., & Roche, P. F. 1982, *MNRAS*, 200, 217
- Asplund, M., Grevesse, N., & Sauval, A. J. 2005, *ASP Conf. Ser.*, ed. Bash & Barnes, 336
- Bains, I., Redman, M. P., Bryce, M., & Meaburn, J. 2004, *MNRAS*, 354, 549
- Benjamin, R. A., Skillman, E. D., & Smits, D. P. 1999, *ApJ*, 514, 307
- Bernard Salas, J., Pottasch, S. R., Beintema, D. A., & Wesselius, P. R. 2001, *A&A*, 367, 949
- Ferland, G. J., Korista, K. T., Verner, D. A., et al. 1998, *PASP*, 110, 761
- Fluks, M. A., Plez, B., de Winter, D., et al. 1994, *A&AS*, 105, 311
- Guerrero, M. A., Chu, Y.-H., & Miranda, L. F. 2004, *AJ*, 128, 1694
- Hummer, D. G., & Storey, P. J. 1987, *MNRAS*, 224, 801
- Kastner, J. H., Balick, B., Blackman, E. G., et al. 2003, *ApJ*, 591, L37
- Kurucz, R. L. 1991, in *Proc. of the Workshop on Precision Photometry: Astrophysics of the Galaxy*, ed. A. C. Davis Philip, A. R. Upgren, & K. A. James (Schenectady: Davis), 27
- Lagage, P. O., Pel, J. W., Authier, M., et al. 2004, *Messenger*, 117, 12
- Liu, X.-W., Barlow, M. J., Cohen, M., et al. 2001, *MNRAS*, 323, 343
- Lucke, P. B. 1978, *A&A*, 64, 367
- Pottasch, S. R., & Acker, A. 1989, *A&A*, 221, 123
- Pottasch, S. R., & Beintema, D. A. 1999, *A&A*, 347, 975
- Pottasch, S. R., & Surendiranath, R. 2005, *A&A*, 432, 139
- Pottasch, S. R., Wesselius, P. R., Wu, C. C., et al. 1977, *A&A*, 54, 435
- Pottasch, S. R., Preite-Martinez, A., Olon, F. M., et al. 1986, *A&A*, 161, 363
- Pottasch, S. R., Beintema, D. A., & Feibelman, W. A. 2000, *A&A*, 363, 767
- Pottasch, S. R., Beintema, D. A., Bernard Salas, J., & Feibelman, W. A. 2001, *A&A*, 380, 684
- Pottasch, S. R., Beintema, D. A., Bernard Salas, J., et al. 2002, *A&A*, 393, 285
- Preite-Martinez, A., & Pottasch, S. R. 1983, *A&A*, 126, 31
- Redman, M. P., O'Connor, J. A., Holloway, J. A., et al. 2000, *MNRAS*, 312, L23
- Santander-Garcia, M., Corradi, R. L. M., Balick, B., & Mampaso, A. 2004, *A&A*, 426, 185
- Seaton, M. J. 1979, *MNRAS*, 187, 73P
- Smith, N. 2003, *MNRAS*, 342, 383
- Smith, N., & Gehr, R. D. 2005, *AJ*, 129, 969
- Surendiranath, R., Pottasch, S. R., & García-Lario, P. 2004, *A&A*, 421, 1051
- Wang, W., Liu, X.-W., Zhang, Y., & Barlow, M. J. 2004, *A&A*, 427, 873
- Webster, B. L. 1969, *MNRAS*, 143, 79
- Zhang, Y., & Liu, X.-W. 2002, *MNRAS*, 337, 499